

DOI: 10.1070/QEL16053

Analytical description of attosecond pulse generation on a plasma surface irradiated by high-intense laser pulses

M. Cherednychek, A. Pukhov

Abstract. **We study theoretically the process of turning a laser pulse into a train of attosecond or even zeptosecond pulses due to high harmonic generation (HHG) upon backreflection of intense laser radiation from a plasma surface. It is shown that under appropriate conditions these attosecond pulses may have an amplitude that is several orders of magnitude larger than that of the laser pulse. We study this process in detail, especially the nanobunching of the plasma electron density. We derive the analytical expression that describes the electron density profile and obtain a good agreement with particle-in-cell simulations. We investigate the most efficient case of HHG at a moderate laser intensity (normalised vector potential $a_0 = 10$) on the overdense plasma slab with an exponential pre-plasma profile. Subsequently we calculate the spectra of single attosecond pulses from back radiation using our expression for density shape in combination with the equation for spectrum of nanobunch radiation.**

Keywords: *high harmonic generation, attosecond pulses, plasma surface.*

1. Introduction

In last decade the development of laser technology has shown an immense progress [1–4], which opens an opportunity to study the new physical phenomena of laser–plasma interaction. One of the most important processes in this field is the high harmonic generation (HHG), which is being studied very intensely today. As the minimum achievable duration of laser pulses is reducing with time, it is interesting whether the generation of even shorter pulses (in attosecond or even zeptosecond range) is possible. The reduction of the pulse duration and the radiation wavelength would open new potential applications, which is the motivation of the HHG investigation.

The most efficient method of HHG is the interaction of high contrast laser pulses [5] with solid density targets. The pedestal of the pulse ionises the surface and the main pulse interacts with overdense plasma electrons, while ions remain virtually immobile during the short pulse duration. One distinguishes two main HHG mechanisms in this case: coherent wake emission (CWE) [5,6] and relativistically oscillating mirror (ROM) [7–11]. CWE is caused by fast Brunel electrons [12] which excite the plasma oscillations at the local plasma frequencies. Thus there is no harmonics behind the maximal plasma frequency in the case of CWE. This process dominates for non-relativistic laser intensities, for which the normalised vector potential is $a_0 < 1$.

For $a_0 \gg 1$ the harmonics are generated mostly via ROM. In this case the electron layer at the plasma surface acts as a mirror that oscillates at relativistic velocities and generates high order harmonics via the Doppler effect, while moving towards the incident wave. For this process there is no limit of frequency like by CWE, and so higher harmonics can be generated. The first theoretical description of ROM claimed that the intensity spectrum envelope of the reflected wave can be described by $I(l) \propto l^{-5/2}$ up to the 'roll over' frequency ω_r proportional to $4\gamma^2$, where l is the harmonic order and γ is the relativistic gamma factor [7]. Later this theory was improved, especially the acceleration of the reflecting layer was taken into account. This results in the power law $I(l) \propto l^{-8/3}$ and $\omega_r \propto \gamma^3$ [8]. This model assumes the existence of a so-called apparent reflection point (ARP) where the transverse electric field vanishes. This model was experimentally proved [9–11].

Most recently another HHG mechanism was discovered. Using a p-polarised oblique incident pulse with $a_0 \gg 1$ one can cause the formation of extremely dense electron nanobunches under appropriate conditions. These bunches emit attosecond pulses with intensities much larger than those of incident pulses [13,14]. That means that the boundary condition assumed in [8] corresponding to the ARP fails and thus the ROM theory cannot be applied in this case. This process is called coherent synchrotron emission (CSE). The reflected radiation in case of CSE is characterised by the power law $I(l) \propto l^{-4/3}$ or $I(l) \propto l^{-6/5}$ which is flatter as compared to ROM [13,14]. The corresponding experiments can be found in Refs [15–17].

Detailed numerical investigation of the case of p-polarised oblique incidence in Ref. [18] shows that the ROM model can be violated when the similarity parameter $S = n/a_0$ (where n is the electron density given in units of the critical density n_c [19]) is smaller than five. The authors of [18] present a new relativistic electronic spring (RES) model for $S < 5$.

In this work we investigate the CSE process described in [13,14] more extensively. We introduce an original analytical approach which allows us to calculate the electron density profile of the given nanobunch as well as its current distribution. The obtained equations enable us to improve the formulas for a back-radiating spectrum derived in [13,14]. Moreover we perform several 1D PIC simulations and find different regimes of HHG. Finally we compare the derived expressions with simulation results done with 1D PIC-code called VLPL.

M. Cherednychek, A. Pukhov Institut für theoretische Physik, Heinrich-Heine-Universität Düsseldorf, 40225 Düsseldorf, Deutschland; e-mail: pukhov@tp1.uni-duesseldorf.de

Received 5 February 2016
Kvantovaya Elektronika **46** (4) 353–360 (2016)
Submitted in English

2. PIC simulation of the HHG process

For our simulations we use a one dimensional version of the PIC code called Virtual Laser Plasma Laboratory (VLPL) [20]. In our geometry the incident wave comes from the left hand side of the simulation box and propagates along the x axis. The wave is p-polarised and the electric field component oscillates along the y axis. The plasma is located at the right hand side of the simulation box. It is also possible to describe the interactions where oblique incidence is used with our code. Let θ be the angle of incidence in the laboratory frame. We consider some frame moving along the y axis with velocity $V = c\sin\theta$. The Lorenz transforms verify that in this frame the laser radiation is normally incident (see [21] for more details). At the same time the whole plasma moves in the y direction in this frame. Thus, attributing some initial velocity to plasma in our simulation we are working in the moving frame. If we need the results in the laboratory frame, we have to transform the values obtained from the simulation via the Lorenz transform. Consequently we obtain the results that correspond to the process with oblique incidence. We use the incident field $E_i(t)$ of duration $T = 10\lambda/c$ that is given by the expression

$$E_i(t) = \frac{1}{4}\left[1 + \tanh\left(\frac{t}{\Delta t}\right)\right]\left[1 - \tanh\left(\frac{t-T}{\Delta t}\right)\right]\sin(2\pi t),$$

where $\Delta t = \lambda/4$. Below we use the plasma exponential density ramp for $x < 0$. For $x > 0$ the density remains constant:

$$n(x) = \begin{cases} n_0 \exp(x/\sigma) & \text{for } x < 0, \\ n_0 & \text{for } x > 0. \end{cases} \quad (1)$$

Assuming that the ions are at rest during the whole interaction process we consider only the interaction between the electrons and the incident wave. In the simple case of normal incidence there are two forces acting on particles along the x axis: the electrostatic force proportional to E_x and laser ponderomotive force oscillating with 2ω (twice the laser frequency). Thus the plasma surface oscillates with half the laser period. In the case of oblique incidence of a p-polarised wave there is an additional longitudinal component of the electric field oscillating at frequency ω and acting on surface. Consequently the interaction becomes even more complicated which leads to stronger oscillations on the plasma surface containing both ω and 2ω modes.

Thus, as soon as the electrons are pulled back by the electrostatic force they form a thin nanobunch that reaches a velocity close to c. In this case the generation of high harmonics is possible.

3. Density profile of a thin electron layer

In this section we derive two different analytic expressions for two different cases, which roughly describe the electron density profile at the intervals where sharp spikes appear. The starting point of our calculations is the approximation of the electron phase space distribution at these intervals. As we will see later this distribution depends on the propagation velocity $\dot{x}_0(t)$ of the given electron layer.

Firstly let us consider the case of a slow electron bunch [$\dot{x}_0(t) \ll c$]. Figure 1 shows the electron density and its distribution in the $x-p_x$ phase space at a certain time. Let the curve in phase space be described by the function $x(p)$ at some small

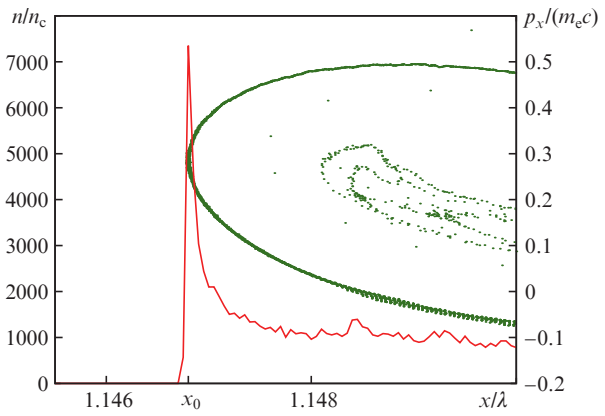

Figure 1. (Colour online) Electron density (red) and electrons in $x-p_x$ plane (green); x_0 is the position of the maximal density. Simulation parameters: initial plasma density $n_0 = 38.9n_c$; $\sigma = 1.1836\times10^{-3}\lambda$ (laboratory frame), a 820-nm pulse with a dimensionless amplitude $a_0 = 10$ and p-polarised oblique incidence at 57°.

interval close to the density spike. Obviously, x_0 is the local minimum of this function that coincides with the position of the spike. In fact, we have always a spike of electron density at the point, where the function $x(p)$ exhibits the local extreme value. The idea that gives us the starting point for our calculations is the following. We can locally describe the given curve in phase space as a parabola:

$$x(p,t) = x_0(t) + \alpha(t)(p - p_0(t))^2. \quad (2)$$

The point $[x_0(t), p_0(t)]$ corresponds to the local minimum. In order to simplify the notation, we drop the time dependence and set $p_0 = x_0 = 0$. Then we have

$$x(p) = \alpha p^2.$$

We consider some short interval Δx where this assumption makes sense. The distribution function of the electrons is then given by

$$f_a(x,p) = C\delta_a(x - \alpha p^2), \quad (3)$$

where C is a normalisation constant and δ_a is defined as

$$\delta_a(x) \equiv \begin{cases} g_a(x) & \text{for } x \in [-a,a], \\ 0 & \text{otherwise,} \end{cases}$$

with the property

$$\lim_{a\to 0} \delta_a(x) = \delta(x), \quad (4)$$

where

$$g_a(x) \equiv \frac{3}{4a}\left(1 - \frac{x^2}{a^2}\right).$$

The parameter a describes the width of δ_a, which means that $a > 0$ is required. In order to get the expression for the density we have to perform the integration in the momentum space

$$n_a(x) = \int f_a(x,p)\,dp. \quad (5)$$

We have to be careful with integration boundaries since δ_a is the bounded support function. As a result we obtain:

$$n_a(x) = \begin{cases} \dfrac{2C}{5a^3\sqrt{\alpha}}(3a^2 - 2x^2 - ax)\sqrt{x+a} \quad \text{for } x \in [-a,a], \\ \dfrac{2C}{5a^3\sqrt{\alpha}}[(3a^2 - 2x^2)(\sqrt{x+a} - \sqrt{x-a}) \\ \qquad + ax(\sqrt{x+a} + \sqrt{x-a})] \quad \text{for } x > a, \\ 0 \quad \text{for } x < -a. \end{cases} \tag{6}$$

In order to calculate the constant C, we first write an equation for the number of particles in the interval $[-a, \Delta x]$ by integrating the density over this interval:

$$N_{a,\Delta x} = C\int_{-a}^{\Delta x} n_a(x)\,\mathrm{d}x \overset{a \ll \Delta x}{=} 2C\sqrt{\Delta x/\alpha}\,. \tag{7}$$

Further we solve the obtained equation for C and insert it into equation (6). Finally we obtain the expression for the electron density profile

$$n_a(x) = \begin{cases} \dfrac{N_{a,\Delta x}}{5a^3\sqrt{\Delta x}}(3a^2 - 2x^2 - ax)\sqrt{x+a} \\ \qquad \text{for } x \in [-a,a], \\ \dfrac{N_{a,\Delta x}}{5a^3\sqrt{\Delta x}}[(3a^2 - 2x^2)(\sqrt{x+a} - \sqrt{x-a}) \\ \qquad + ax(\sqrt{x+a} + \sqrt{x-a})] \quad \text{for } x > a, \\ 0 \quad \text{for } x < -a. \end{cases} \tag{8}$$

Note that the parameter α is reduced and does not affect the density profile. In Fig. 2 we see that the density described by (8) agrees very well with the simulation results. We call the case where $\dot{x}_0(t) \ll c$ is valid, the 'parabolic case'. We chose quite a small value for a because we are dealing with a very big and sharp spike in this example. This is due to a strong laser pulse and very small cell size ($5\times10^{-5}\lambda$).

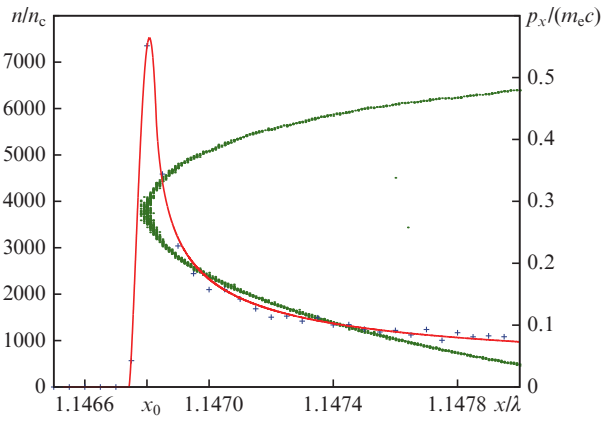

Figure 2. (Colour online) Electron density taken from the simulation (blue) and calculated analytically by (8) (red), with same simulation parameters as those in Fig. 1; $\Delta x = 0.0012\lambda$, $a = 4.4\times10^{-5}$ (simulation frame).

Now we discuss another case with $\dot{x}_0(t) \to c$. Consider the phase space evolution taken from another simulation illustrated in Fig. 3. At the beginning by $t = 5.4\lambda/c$ the momentum is close to zero and the distribution is parabolic as expected. Further, as soon as the electron bunch is pulled back by the electrostatic force, the negative momentum of the bunch growth constantly with time and the distribution changes resembling a kind of 'whip' between $t = 5.7\lambda/c$ and $5.8\lambda/c$. The extremely dense electron nanobunch reaches the velocity close to c during this period. In this case the phase space distribution can be roughly fitted with an exponential function

$$x_p(p,t) = x_0(t) + \exp[\alpha(t)(p - p_0(t))]. \tag{9}$$

As we will show later the incident angle and the density gradient used here are optimal for producing the most intense attosecond pulse. The given phase space distribution belongs to the nanobunch that radiates this pulse. As in the previous

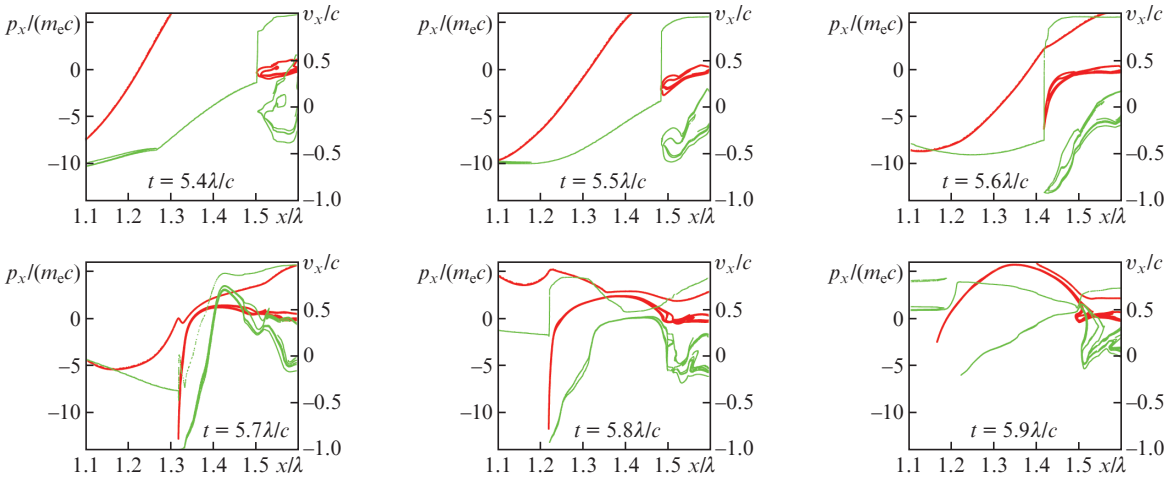

Figure 3. (Colour online) Electrons in x–p_x plane (red) and its longitudinal velocity (green) taken from the simulation at different times t during the process of nanobunching at $n_0 = 100n_c$; $\sigma = 0.4\lambda_c$ (laboratory frame), a 820-nm pulse with a dimensionless amplitude $a_0 = 10$ and p-polarised oblique incidence at 50°.

case we drop the time dependence and set $p_0 = x_0 = 0$. Then we have

$$x_p(p) = \exp(\alpha p) \tag{10}$$

and the distribution function:

$$f_a(x,p) = C\delta_a(x - \exp(\alpha p)). \tag{11}$$

The density can be given in this case by

$$n_a(x) = \int_{-p_{\text{cut}}} f_a(x,p)\,\mathrm{d}p, \tag{12}$$

since we should take into account that the momentum of the electrons is limited by some amount p_{cut}. Further we calculate the number of particles on some interval $[x_{\min}, x_{\max}]$, where $x_{\min} = \exp(-\alpha p_{\text{cut}})$, in order to obtain the normalisation constant C. Finally, we obtain:

$$n_a(x) = \begin{cases} \dfrac{3N}{4a^3\ln(x_{\max}/x_{\min})}\left\{(x+a)\left[x + (x-a)\left[\dfrac{1}{2} + \ln\left(\dfrac{x_{\min}}{x+a}\right)\right]\right]\right. \\ \qquad \left. + x_{\min}\left(\dfrac{1}{2}x_{\min} - 2x\right)\right\} \quad \text{for } x \in [x_{\min} - a, x_{\min} + a], \\ \dfrac{3N}{4a^3\ln(x_{\max}/x_{\min})}\left(2ax - (x^2 - a^2)\ln\left(\dfrac{x+a}{x-a}\right)\right) \\ \qquad \text{for } x > x_{\min} + a, \\ 0 \quad \text{for } x < x_{\min} - a. \end{cases} \tag{13}$$

Now as in the previous case we are going to compare the calculated analytical function with the simulated density profile (Fig. 4). Again we obtain a good agreement and are able to describe the density spike quite well. Although there is some further spike at $x = 1.323\lambda$ which is not described analytically, it does not contribute to the radiation significantly and so we can just ignore it.

Before we go further to the next section we analyse the intermediate case $\dot{x}_0(t) \lesssim c$, which is important for further applications. In this case the electron phase space distribution looks like that shown in Fig. 5 and cannot be approximated well either with a parabolic or with an exponential function. Nevertheless, we find out that the density profile of the spike can still be well approximated with equation (8) (Fig. 5), and so we classify the cases with intermediate velocities as parabolic.

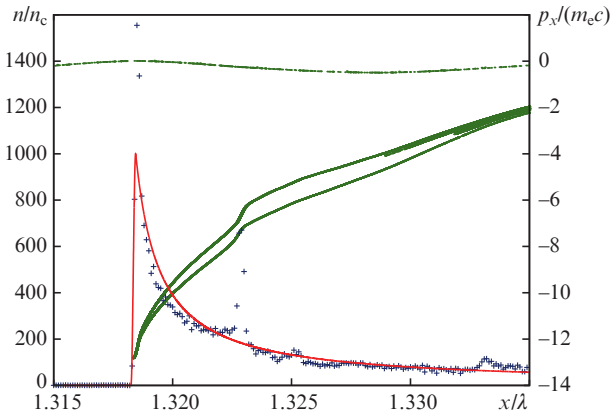

Figure 4. (Colour online) Electron density taken from the simulation (blue) and calculated analytically by (13) (red), as well as electrons in the $x-p_x$ plane (green), with the same simulation parameters as in Fig. 3, taken at $t = 5.7\lambda/c$, $x_{\min} - x_0 = 9\times10^{-4}\lambda$, $x_{\max} - x_0 = 0.02\lambda$, $a = 1\times10^{-4}$ (simulation frame).

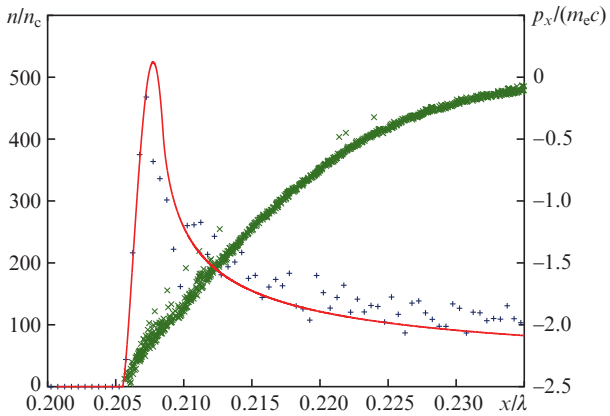

Figure 5. (Colour online) Electron density taken from the simulation (blue) and calculated analytically by (8) (red), as well as electrons in the $x-p_x$ plane (green). Simulation parameters: $n_0 = 100n_c$; $\sigma = 0.066\lambda$ (laboratory frame), a 820-nm pulse with a dimensionless amplitude $a_0 = 10$ and p-polarised oblique incidence at 60°.

In Section 4 we are going to analyse the corresponding simulation results more extensively. We will use the descriptions of the electron layer density profile derived here in order to calculate an expression for the spectra of the reflected waves in different cases.

4. Electron density evolution and HHG

We are interested in the high-frequency spectrum of the reflected pulse mostly determined by the behaviour of the ARP when it moves away from plasma with a maximal velocity. This moment corresponds to a stationary phase point (SPP) (see [13, 14]). The ARP gamma factor exhibits a sharp spike at this time, which is called γ-spike [8]. One distinguish different orders of γ-spikes depending on the behaviour of the transverse current $j_\perp$ in the vicinity of the SPP, which can be approximated with

$$j_\perp(t,x) \approx (-\alpha_0 t)^n f(x - x_0(t)). \tag{14}$$

We assume that the transverse current density does not change its shape f during the time. The number j denotes the order of the given γ-spike. The reflected radiation is determined by the transverse current distribution via

$$E_r(t) = \pi\int j_\perp(t - x, x)\,\mathrm{d}x, \tag{15}$$

and so we are able to derive the expression for the spectrum of the reflected pulse in line with [16] and obtain:

$$I(\omega) = 4\pi^4\alpha_0^2(\alpha_1\omega)^{-\frac{2n+2}{2n+1}}\left(\frac{\mathrm{d}^j}{\mathrm{d}\xi^j}\,\mathrm{Ai}_j(\xi_j)\right)^2 |f(\omega)|^2,$$

where

$$\xi_j = \alpha_1^{-\frac{1}{2j+1}}\delta\omega^{\frac{2j}{2j+1}}; \quad \mathrm{Ai}_j = \frac{1}{2\pi}\int\exp\left[\mathrm{i}\left(xt + \frac{t^{2j+1}}{2j+1}\right)\right]\mathrm{d}t; \tag{16}$$

$$\alpha_1 = \frac{a_0^2}{2vn_{\max}^2}; \quad \delta = 1 - v_{\max};$$

where $v_{\max}$ is the maximal velocity of the moving electron layer in the SPP; and $n_{\max}$ is the maximal density assumed to be constant in time. In (15) we use the normalised PIC units [22]. To give the expression for the shape function we use the results from the previous section and write

$$f(x) = \frac{n_a(x)}{n_a(x_{\max})} \exp(-x^2/\tilde{\sigma}^2), \quad n_a(x_{\max}) = n_{\max}. \tag{17}$$

We multiply the density profile with a wider Gaussian function since n_a decays too slowly (as $\propto 1/x$ for a 'whip' or as $\propto 1/\sqrt{x}$ for a parabolic case) for positive x and after certain x value does not coincide with the given density.

Further we consider two different examples where we apply (16) to calculate the spectrum of a single reflected pulse $E_r^p(t)$, that is filtered out by the Gaussian function

$$E_r^p(t) = E_r(t) \exp[(t - t_{\max})^2/\tilde{\sigma}^2], \tag{18}$$

where $t_{\max}$ corresponds to the maximal wave amplitude and $\tilde{\sigma} = 0.2\lambda/c$.

At first we investigate the example of the whip case [$\dot{x}_0(t) \to c$] from the previous section illustrated in Figs 3 and 4. The electron nanobunch which radiates a strong attosecond pulse can be clearly recognised from Figs 6 and 7a. For convenience we chose the coordinates in the way that the SPP is at point (0, 0). In Fig. 8b the spectrum calculated using (16) is compared with the spectrum calculated from original reflected pulse via the fast Fourier transform. Obviously, the description works well almost until 1000th harmonic. In Fig. 8a the corresponding pulses are compared. The both graphs behave in the similar manner.

Going along the same lines we analyse now the intermediate case [$\dot{x}_0(t) \lesssim c$] shown in Fig. 5. As we said before we attribute this case to the parabolic case. The corresponding pictures illustrating this case are Figs 9, 10 and 11. Here the velocity in SPP significantly deviates from the speed of light and approximately equals $0.91c$. For that reason the electron phase space distribution does not become 'whip-like' (Fig. 5). Although there is no ultrarelativistic regime here, we still may apply the same analysis, assuming the absolute velocity of the electrons to be approximately constant close to SPP. Again we obtain good agreement for the spectrum behavior.

We see that in the first example (whip case) we have the second order gamma spike, whereas in the second example (parabolic case) the first order gamma spike is obtained. In order to find the parameter ranges which correspond to a whip or a parabolic case we perform a number of simulations. Using a moderate intensity of an incident wave ($a_0 = 10$) we vary the steepness of the exponential density gradient as well as the incident angle. For each parameter set we consider the

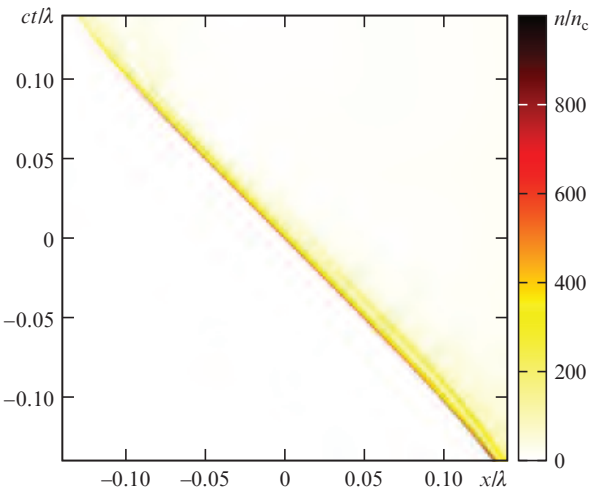

Figure 6. (Colour online) Electron density distribution of the radiating nanobunch in a space time domain. Simulation parameters are the same as in Fig. 3; the SPP [here (0,0)] corresponds to $t = 5.7\lambda/c$ as in Fig. 4.

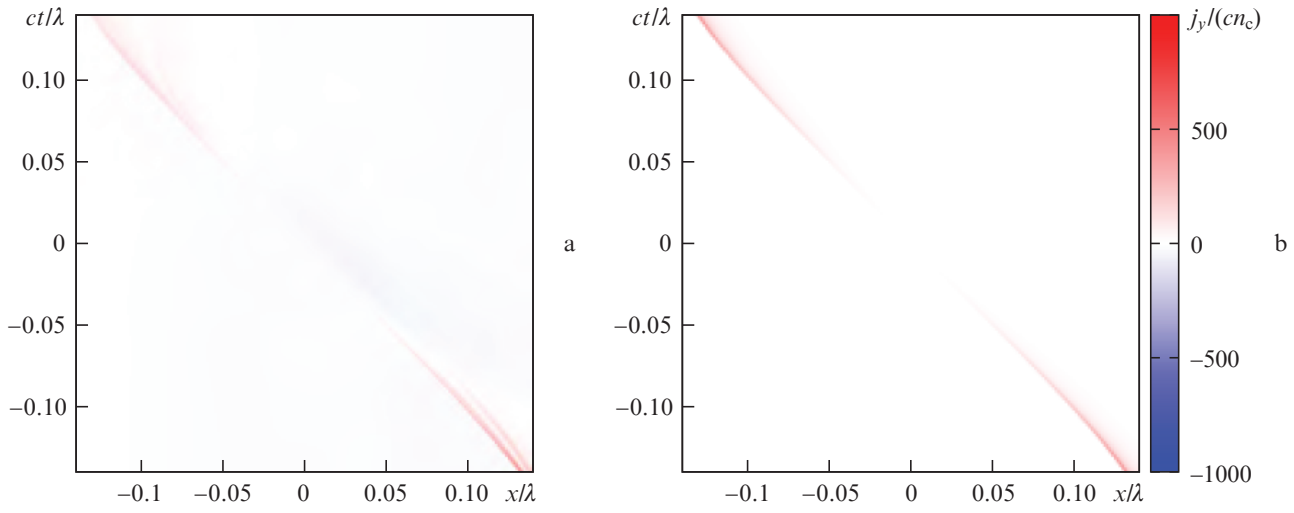

Figure 7. (Colour online) Transverse current density from the simulation near the SPP (0,0) (a) and calculated analytically by (14) at $n = 2$ (b). Simulation parameters are the same as in Fig. 3. The parameters used by the analytical calculation for $x_0(t)$: $\alpha_0 = 4\times10^4$, $n_{\max} = 1000$ and $\gamma = 15$; for shape: $a = 1\times10^{-4}\lambda$, $x_{\min} = 9\times10^{-4}\lambda$ and $\tilde{\sigma} = 0.02\lambda$. The velocity v is derived from the given gamma factor. The Fourier transform of the shape function $f(\omega)$ is calculated numerically using the FFT.

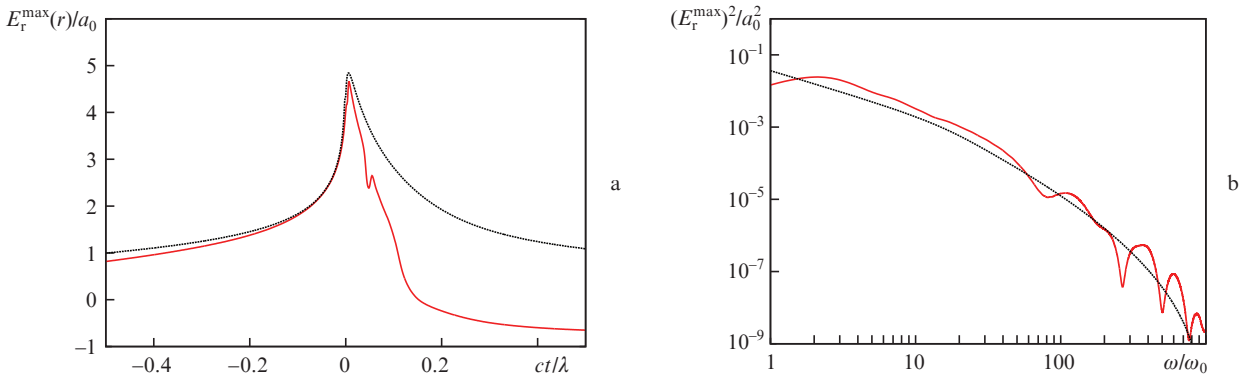

Figure 8. (Colour online) Reflected radiation obtained from the simulation [(a), red] and from the analytical current distribution [(a), black], as well as the corresponding spectra in (b). The spectrum from the simulation is taken directly from the radiated pulse via the FFT, while the other one is obtained using equation (16).

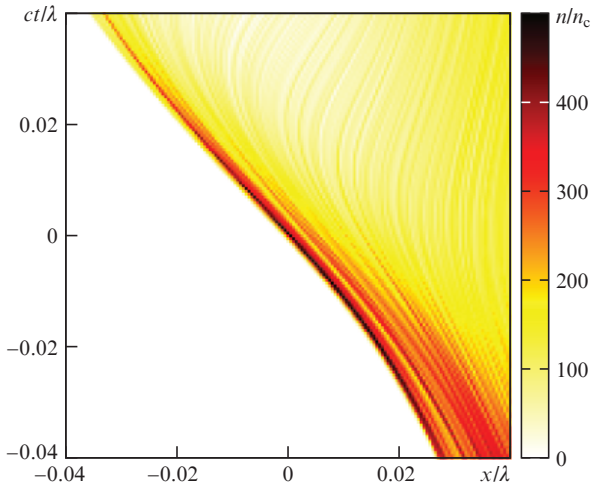

Figure 9. (Colour online) The electron density distribution of the radiating nanobunch in the space time domain. Simulation parameters are the same as those in Fig. 5. The density profile in SPP [here (0,0)] is shown in Fig. 5.

reflected radiation. In Fig. 12 we visualised the maximal amplitude of reflected wave for each parameter set, respectively.

Consider the incidence angle between 45° and 60°, since at these angles the most interesting things occur. Of course we notice a sharp increase in the reflected wave amplitude in the region around $\sigma = 0.4\lambda$. We call this region a high amplitude parameter set (HAPS). In this region we mostly obtain the second order γ-spikes and the current does not change its sign in SPPs like in Fig. 7 Furthermore our study shows that the maximal longitudinal velocity of the certain boundary electron layer increases monotonously with σ up to the HAPS, where it almost reaches c. For $\sigma < 0.05\lambda$ the boundary oscillates too slowly so that no short pulses are generated.

Roughly between 0.05λ and 0.1λ we obtain the reflected radiation similar to Fig. 11. We call this region a moderate amplitude parameter set (MAPS). Here we have only first order γ-spikes and the current changes sign in SPPs (Fig. 10). Thus the reflected spectrum in the MAPS can be approximated with equation (8) (parabolic case) and the region of the HAPS corresponds then to the exponential case [equation

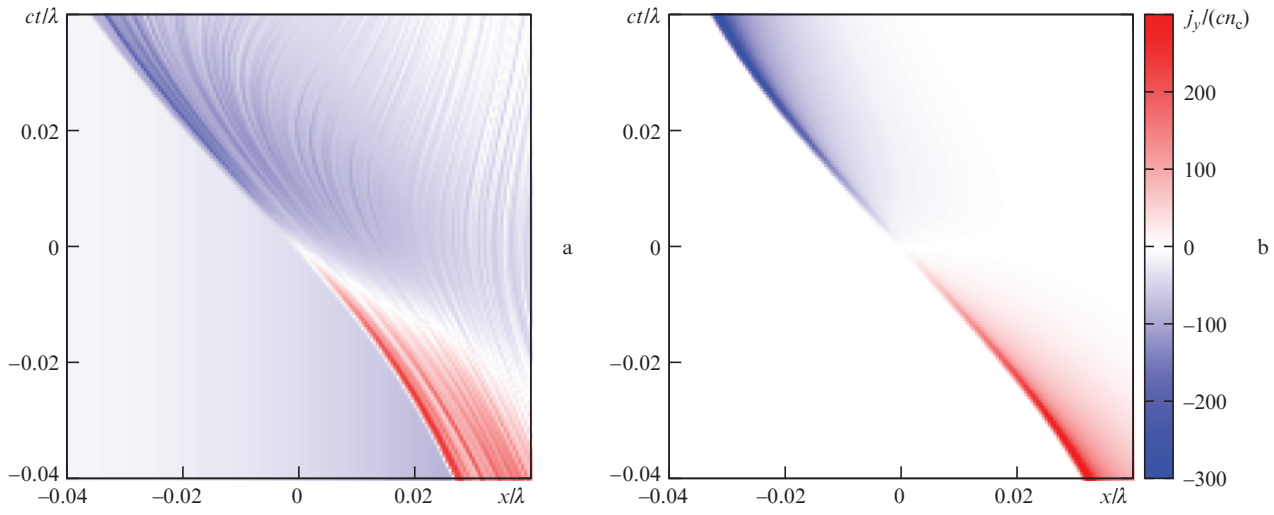

Figure 10. (Colour online) Transverse current density from the simulation near the SPP (a) and calculated analytically by (14) at $n = 1$ (b). Simulation parameters are the same as those in Fig. 5. The parameters used by the analytical calculation for $x_0(t)$: $\alpha_0 = 1\times10^4$, $n_{max} = 500$ and $\gamma = 2.5$; for shape: $a = 1\times10^{-3}\lambda$ and $\tilde{\tilde{\sigma}} = 0.02\lambda$. The velocity v is derived from the given gamma factor.

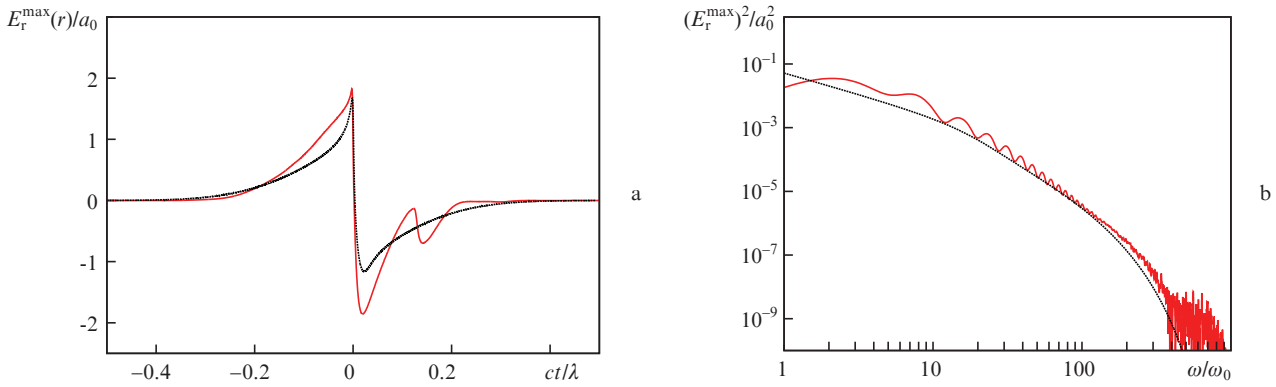

Figure 11. (Colour online) Reflected radiation obtained from the simulation [(a), red] and from the analytical current distribution [(a), black], as well as the corresponding spectra (b).

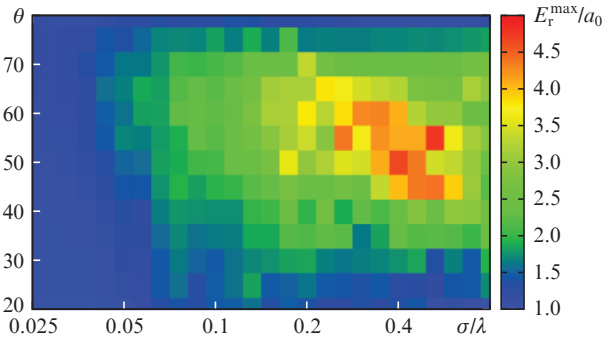

Figure 12. (Colour online) Distribution of the maximum amplitude of reflected radiation in the plane of the incident angle–steepness of the density gradient [σ is taken from (1) and $n_0 = 100\,n_c$]. Each point is obtained in the numerical experiment (laboratory frame).

(13)]. In the region between the MAPS and HAPS the interaction is too complicated to be attributed to any model.

5. Conclusions

We have managed to obtain two different analytical expressions of the electron density profile describing the density spikes in two different cases. We present some simulation results of HHG, where we can obtain the amplitude increasing in the reflected pulse by a factor of five without using an extremely intense incident wave. This is possible after we have found optimal parameters for the density gradient combined with an optimal incident angle. Moreover, with some simple assumptions we have managed to describe analytically the transverse current distribution in the vicinity of SPP in both cases. Obtained expressions together with the expressions for the electron density give us the possibility to reliably calculate the spectra that fit the original spectra of a back radiated pulse.

Our work basically presents the idea of description of the plasma density considering the electron phase space distribution, but this theory has a potential to grow and to be developed further. In this work we have introduced two application examples of our theory. Nevertheless, it can become a strong tool in laser plasma analysis in general.

Acknowledgements. This work has been supported by DFG TR18 and EU FP7 Eucard-2 projects.

References

1. Yanovsky V., Chvykov V., Kalinchenko G., Rousseau P., Planchon T., Matsuoka T., Maksimchuk A., Nees J., Cheriaux G., Mourou G., Krushelnick K. *Opt. Express*, **16**, 2109 (2008).
2. Mourou G.A., Tajima T. *Science*, **331**, 41 (2011).
3. Schwab M.B., Sävert A., Jäckel O., Polz J., Schnell M., Rinck T., Veisz L., Möller M., Hansinger P., Paulus G.G., Kaluza M.C. *Appl. Phys. Lett.*, **103**, 191118 (2013).
4. Mourou G., Mironov S., Khazanov E., Sergeev A. *Eur. Phys. J. Spec. Top.*, **223**, 1181 (2014).
5. Thaury C., Quéré F., Geindre J., Levy A., Ceccotti T., Monot P., Bougeard M., Réau F. *Nature Phys.*, **3**, 424 (2007).
6. Quéré F., Thaury C., Monot P., Dobosz S., Martin P., Geindre J.-P., Audebert P. *Phys. Rev. Lett.*, **96**, 125004 (2006).
7. Gordienko S., Pukhov A., Shorokhov O., Baeva T. *Phys. Rev. Lett.*, **93**, 115002 (2004).
8. Baeva T., Gordienko S., Pukhov A. *Phys. Rev. E*, **74**, 046404 (2006).
9. Dromey B., Zepf M., Gopal A., Lancaster K., Wei M.S., Krushelnick K., Tatarakis M., Vakakis N., Moustaizis S., Kodama R., Tampo M., Stoeckl C., Clarke R., Habara H., Neely D., Karsch S., Norreys P. *Nature Phys.*, **2**, 456 (2006).
10. Dromey B., Kar S., Bellei C., Carroll D.C., Clarke R.J., Green J.S., Kneip S., Markey K., Nagel S.R., Simpson P.T., Willingale L., McKenna P., Neely D., Najmudin Z., Krushelnick K., Norreys P.A., Zepf M. *Phys. Rev. Lett.*, **99**, 085001 (2007).
11. Heissler P., Hörlein R., Mikhailova J.M., Waldecker L., Tzallas P., Buck A., Schmid K., Sears C.M.S., Krausz F., Veisz L., Zepf M., Tsakiris G.D. *Phys. Rev. Lett.*, **108**, 235003 (2012).
12. Brunel F. *Phys. Rev. Lett.*, **59**, 52 (1987).
13. an der Brügge D., Pukhov A. *Phys. Plasmas*, **17**, 033110 (2010).
14. an der Brügge D., Pukhov A. e-print arXiv:physics/1111.4133.
15. Dromey B., Rykovanov M.S., Yeung M., Horlein R., Jung D., Gautier D.C., Dzelzainis T., Kiefer D., Palaniyppan S., Shah R., Schreiber J., Ruhl H., Fernandez J.C., Lewis C.L.S., Zepf M., Hegelich B.M. *Nature Phys.*, **8**, 804 (2012).
16. Dromey B., Cousens S., Rykovanov S., Yeung M., Jung D., Gautier D.C., Dzelzainis T., Kiefer D., Palaniyppan S., Shah R., Schreiber J., Fernandez J.C., Lewis C.L.S., Zepf M., Hegelich B.M. *New J. Phys.*, **15**, 015025 (2013).
17. Yeung M., Dromey B., Cousens S., Dzelzainis T., Kiefer D., Schreiber J., Bin J.H., Ma W., Kreuzer C., Meyerter-Vehn J., Streeter M.J.V., Foster P.S., Rykovanov S., Zepf M. *Phys. Rev. Lett.*, **122**, 123902 (2014).
18. Gonoskov A.A., Korzhimanov A.V., Kim A.V., Marklund M., Sergeev A.M. *Phys. Rev. E*, **84**, 046403 (2011).

19. Gordienko S., Pukhov A. *Phys. Plasmas*, **12**, 043109 (2005).
20. Pukhov A. *J. Plasma Phys*., **61**, 425 (1999).
21. Landau L.D., Lifshitz E.M. *The Classical Theory of Fields* (Pergamon, New York, 1964).
22. Wu H.-C. e-print arXiv:physics/1104.3163.